

SF1-specific deletion of the energy sensor AMPK γ 2 induces obesity



Óscar Freire-Agulleiro^{1,2}, Ánxela Estévez-Salguero^{1,2}, Vitor Ferreira^{1,2}, Cassie Lynn Holleman^{3,4}, Julia García-Currás⁵, Ismael González-García^{1,2}, Rubén Nogueiras^{1,2}, Manuel Tena-Sempere^{2,6}, Cristina García-Cáceres^{3,4,7}, Carlos Diéguez^{1,2}, Miguel López^{1,2,*}

ABSTRACT

Objective: AMP-activated protein kinase (AMPK) is a heterotrimer complex consisting of a catalytic α subunit (α 1, α 2) with a serine/threonine kinase domain, and two regulatory subunits, β (β 1, β 2) and γ (γ 1, γ 2, γ 3), encoded by different genes. In the hypothalamus, AMPK plays a crucial role in regulating energy balance, including feeding, energy expenditure, peripheral glucose and lipid metabolism. However, most research on hypothalamic AMPK has concentrated on the catalytic subunits AMPK α 1 and AMPK α 2, with little focus on the regulatory subunits.

Methods: To fill this gap of knowledge, we investigated the effects of selectively deleting the regulatory isoform AMPK γ 2, which is a primary “energy sensor”, in steroidogenic factor 1 (SF1) neurons of the ventromedial hypothalamic nucleus (VMH). Complete metabolic phenotyping and molecular analyses in brown adipose tissue (BAT), white adipose tissue (WAT) and liver were carried out.

Results: Our findings reveal that, in contrast to the obesity-protective effect of the genetic deletion of AMPK α subunits, the loss of AMPK γ 2 in SF1 neurons leads to a sex-independent and feeding-independent obesity-prone phenotype due to decreased thermogenesis in brown adipose tissue (BAT) and reduced browning of WAT, resulting in lower energy expenditure. Additionally, SF1-Cre AMPK γ 2 mice exhibit hepatic lipid accumulation, but surprisingly maintain normal glucose homeostasis.

Conclusions: Overall, these results highlight the distinct roles of AMPK subunits within the hypothalamus.

© 2024 The Author(s). Published by Elsevier GmbH. This is an open access article under the CC BY-NC-ND license (<http://creativecommons.org/licenses/by-nc-nd/4.0/>).

Keywords AMPK; BAT; Hypothalamus; Obesity; SF1; Thermogenesis

1. INTRODUCTION

Adenosine monophosphate-activated protein kinase (AMPK) is an evolutionarily highly conserved serine/threonine kinase, with orthologues in all kingdoms of the domain Eukarya [1–5]. At the molecular level, AMPK is a heterotrimer complex comprising a catalytic α subunit, with a conventional serine/threonine kinase domain, and two regulatory subunits, β and γ , encoded by different genes. There are two isoforms of the α (α 1, α 2) and β (β 1, β 2) subunits and three isoforms of the γ subunit (γ 1, γ 2, γ 3), giving rise to twelve possible combinations of the heterotrimeric $\alpha\beta\gamma$ AMPK complex [1–5]. AMPK is activated by phosphorylation of Thr172 of the α subunit, a process that can be regulated by several mechanisms, such as upstream liver kinase B1 (LKB1) and calmodulin-dependent kinase kinase 2 (CaMKK2; also known as CaMKK β), an increase in the intracellular calcium ions, (which is mediated by CAMKK2), and by a decrease in fructose 1,6-bisphosphate (FBP), a glycolytic intermediate [1–5]. However, the canonical mechanism for allosteric AMPK activation, as

its name suggests, is the binding of adenosine monophosphate (AMP; which rise is associated to low intracellular energy levels) to the γ subunits [1–5]. Therefore, AMPK is a cellular gauge that is activated in conditions of low energy promoting counterregulatory responses. Once activated, AMPK inhibits ATP-consuming processes, while activating catabolic processes. The overall effect of AMPK activation is therefore to produce ATP, thereby maintaining energy homeostasis [1–5].

The AMPK γ subunits contain two Bateman domains, each comprising two cystathionine- β -synthase (CBS) motifs that bind AMP, ADP, or ATP [2–5]. Although mammals have four potential binding sites, only three are functional, with CBS2 typically remaining unoccupied. Recent models suggest that CBS1 is normally occupied by ATP and CBS4 by AMP, both influencing the CBS3 binding site. CBS3 binds AMP (or ADP) in competition with ATP, making it responsible for detecting small changes in cellular AMP:ATP ratios, and therefore acting as the primary “energy sensor” [2–5]. The physiological relevance of AMPK γ is evidenced by data in humans and mice, with naturally

¹Department of Physiology, CiMUS, University of Santiago de Compostela, Santiago de Compostela, 15782, Spain ²CIBER Fisiopatología de la Obesidad y Nutrición (CIBEROBN), Santiago de Compostela, 15706, Spain ³Institute for Diabetes and Obesity, Helmholtz Diabetes Center, Helmholtz Zentrum München, 85764, Neuherberg, Germany ⁴German Center for Diabetes Research (DZD), 85764, Neuherberg, Germany ⁵Biostattech Advice, Training and Innovation in Biostatistics, S.L, Ames, 15895, Spain ⁶Department of Cell Biology, Physiology and Immunology, University of Córdoba, Instituto Maimónides de Investigación Biomédica (IMIBIC)/Hospital Universitario Reina Sofía, Córdoba, 14004, Spain ⁷Medizinische Klinik und Poliklinik IV, Klinikum der Universität, Ludwig-Maximilians-Universität München, 80336, Munich, Germany

*Corresponding author. Department of Physiology, CiMUS, University of Santiago de Compostela, Santiago de Compostela, 15782, Spain. E-mail: m.lopez@usc.es (M. López).

Received November 29, 2024 • Revision received December 21, 2024 • Accepted December 25, 2024 • Available online 31 December 2024

<https://doi.org/10.1016/j.molmet.2024.102091>

occurring mutations in the $\gamma 2$ subunit causing severe cardiac abnormalities [6–9]. It has been also reported that chronic AMPK activation resulting from mutation of the AMPK $\gamma 2$ subunit led to hyperphagia, obesity and impaired insulin secretion in mice and humans [10].

Despite existing evidence, the precise function of hypothalamic AMPK γ subunits remains elusive. This study aimed to elucidate the role of AMPK $\gamma 2$ in hypothalamic neurons on whole-body energy balance regulation. Our findings demonstrate that genetic ablation of AMPK $\gamma 2$ in steroidogenic factor 1 (SF1) neurons of the ventromedial nucleus (VMH) induces a sex-independent and feeding-independent obesity-prone phenotype. This phenotype is characterized by decreased thermogenesis in brown adipose tissue (BAT) and reduced browning of white adipose tissue (WAT), resulting in lower energy expenditure in male mice. These findings highlight the specific roles of AMPK subunits in hypothalamic energy homeostasis control.

2. MATERIALS AND METHODS

2.1. Animals

To generate VMH-specific SF1 neuron AMPK $\gamma 2$ knockout mice, SF1-Cre mice (Tg(Nr5a1-cre)Lowl/J, catalog number 012462; The Jackson Laboratory) [11,12] were crossed with AMPK $\gamma 2$ floxed mice (B6N.Cg-Prkag2tm1.1Rto/J, catalog number 030979, The Jackson Laboratory) [8]. Through selective breeding and genotyping, crosses were established to produce SF1-Cre AMPK $\gamma 2^{fl/fl}$ animals and AMPK $\gamma 2^{fl/fl}$ animals (control littermates). For histological characterization and validation SF1-Cre AMPK $\gamma 2^{fl/fl}$ were also crossed with Ai14-tdTomato animals (B6.Cg-Gt(ROSA)26Sortm14(CAG-tdTomato)Hze/J, catalog number 007914) in order to obtain SF1-Cre; Ai14-tdTomato. Animal genotyping was performed using primers and PCR protocol provided by The Jackson Laboratory.

The animals were housed under a 12-hour artificial light cycle (08:00 to 20:00), maintaining a controlled temperature (22–24 °C) and humidity (55%). They were provided with free access to standard laboratory chow and tap water. Mice were individually housed, and food intake was monitored for 9 consecutive days. Feeding was analyzed between 22 and 25 weeks of age, when both male and female animals already showed a significant difference in body weight. Average daily food intake for the whole period was plotted. All mice were group-housed, except for periods designated for food intake analyses, thermal challenges, and indirect calorimetry studies. The experiments were conducted in accordance with the International Law on Animal Experimentation and were approved by the USC Ethical Committee (Project ID 15012/2020/010).

2.2. Temperature challenges

For acute cold (4 °C) exposure, animals were monitored for 6 h, with body, tail base, and BAT temperatures recorded hourly. To elucidate the potential role of heat dissipation through the tail base as a thermoregulatory mechanism, we measured tail base temperatures in mice briefly acclimated to sub-thermoneutral (26 °C), thermoneutral (30 °C), or supra-thermoneutral (34 °C) conditions on separate days (3–4 days between exposures) using thermal imaging. Core body temperature was determined by inner ear temperature. Acclimation was achieved using a pre-heated warming plate (surface temperature monitored with a thermal camera) enclosed by a PVC tube, allowing free movement while confining animals to the designated area. After 10 min of exposure, thermal images were taken and rectal temperatures analyzed.

2.3. Glucose and insulin tolerance tests

Basal blood glucose levels were measured after an overnight fast (12 h) for the glucose tolerance test (GTT), and after 6 h for the insulin tolerance test (ITT), with a glucometer (Accu-Chek, Roche). The GTT and ITT were performed after an intraperitoneal injection of 2 g/kg D-glucose (Sigma-Aldrich) or 1 U/kg insulin (Novo Nordisk), respectively. Glucose levels and area under the curve (AUC) values were determined as previously described [12–14]. For the postprandial GTT, animals underwent a 12-hour fast during the dark phase, followed by ad libitum access to their standard diet. Body mass, food intake, and glucose levels were measured at baseline and at 30, 60, 120, and 240 min after refeeding, with additional monitoring of food intake up to 10 h.

2.4. Temperature measurements

Body temperature was measured daily for 7 days with a rectal probe connected to a digital thermometer (BAT-12: Microprobe-Thermometer). Skin temperature surrounding BAT and temperature inner ear and tail base were recorded with a B335 compact infrared thermal imaging camera (FLIR) and analyzed with FLIR Tools software (FLIR Systems), as described [14–16].

2.5. Indirect calorimetry and nuclear magnetic resonance

Animals were analyzed for EE, respiratory exchange ratio (RER), and locomotor activity (LA) using calorimetric systems (TSE Systems and Sable Systems) [11,12,14–17]. For body composition analysis, nuclear magnetic resonance (NMR; EchoMRI) was employed [11,12,14–17].

2.6. Sample processing

Mice were killed by cervical dislocation and decapitation, and tissues [hypothalamus, BAT, subcutaneous, gonadal, and visceral white adipose tissue depots (scWAT, gWAT, and vWAT), liver, adrenal, ovary, pituitary and testis] were immediately homogenized on ice. BAT, sWAT, gWAT, vWAT, and liver were weighed. Samples and serum were stored at –80 °C.

2.7. Biochemical analyses

Hepatic cholesterol and triglycerides (1001314 and 1001092; Spinreact) were measured by spectrophotometry (Invitrogen-ThermoFisher).

2.8. Histological analysis

BAT and sWAT samples were processed as shown [11,16,18]. For the adipocyte area, images were analyzed with Adiposoft plugin in Fiji Software (NIH). BAT sections were used for immunohistochemistry detection of uncoupling protein 1 (UCP1). UCP1-positive cells were quantified with Fiji image analysis software, as described elsewhere [14,18]. Hepatic lipid content was analyzed by Oil Red O staining, as previously reported [11,14,18]. Lipids in Oil Red O-stained sections were quantified using Fiji software (NIH). Three pictures per image section were analyzed for histological analysis.

2.9. BaseScope

To validate the SF1-Cre AMPK $\gamma 2$ model, in situ hybridization for exon 6 of the *Prkag2* gene (flanked by loxP sequences in this model) was performed using BaseScope technology (BaseScope™ Detection Reagent Kit v2-Red, ACD Bio – Biotechnie), which allows detection of short mRNA sequences (50–300 nucleotides). The probe used was BaseScope™ Probe-BA-Mm-Prkag2-zzz-st (Cat 717761). Brain sections from perfused and sucrose-dehydrated animals were cut at 10 μ m in a cryostat, mounted on specific slides (SuperFrost slides, Cat 15438060, Fisher Scientific), and processed following the BaseScope protocol. This included fixation, dehydration, antigen retrieval, protease

treatment, probe hybridization, signal amplification, and detection using Fast RED. Hematoxylin counterstaining was performed for anatomical reference. Images were captured at 10x and 40x magnification using a digital camera (Olympus XC50, Olympus Corporation) from 2 AMPK γ 2^{fl/fl} and 4 SF1-Cre AMPK γ 2^{fl/fl} animals. Between 3 and 4 different brain sections were analyzed for each animal bilaterally.

2.10. Immunofluorescence/immunohistochemistry

Adult male mice were transcardially perfused with a saline solution followed by 4% neutral buffered paraformaldehyde (PFA). Brains were dissected and post-fixed for 24 h with 4% PFA, followed by immersion in a 30% sucrose solution for dehydration. When brains sunk, they were sectioned at 30 μ m on a cryostat (Leica Biosystems). Brain sections were incubated with primary antibody (Goat anti-GFAP, 1:1000; Sigma-Aldrich #SAB2500462; RRID: AB_10603437) overnight at 4 °C diluted in 0.1M TBS containing gelatin (0,25%) and Triton X100 (0,5%). Sections were washed with 0,1M TBS and incubated with secondary antibody (Alexa Fluor 488 donkey anti-goat, 1:1000; Invitrogen; A-11055; RRID: AB_2534102) for 2 h at room temperature with 0,1 M TBS containing gelatin (0,25%) and Triton X100 (0,5%). Images were obtained using a Leica TCA SP-8-X Confocal Microscope (Leica Microsystems), and analysis were performed using Fiji 2.0.0 (ImageJ; NIH). Mean intensity values of GFAP immunostaining were acquired for ARC and VMH in 6 brains slices (2 anterior, 2 medial, and 2 posterior hypothalamic regions).

2.11. RT-PCR

Quantitative Real-time PCR (TaqMan®; Applied Biosystems) was conducted as previously outlined [14,16], using commercially available validated TaqMan® probes (ThermoFisher) for AMPK γ 2 (*Prkag2*; assay ID Mm00513968_m1), agouti-related peptide (*AgRP*; assay ID: Mm0475829_g1), neuropeptide Y (*Npy*; assay ID: Mm01410146_m1), proopiomelanocortin (*Pomc*; assay ID: Mm00435874_m1), diacylglycerol o-acyltransferase 1 (*Dgat1*; assay ID: Mm00515643_m1), *Lipin1* (*Lpin1*; assay ID: Mm00550511_m1), and monoacylglycerol o-acyltransferase 1 (*Mogat1*; assay ID: Mm00503358_m1). Values were expressed relative to hypoxanthine-guanine phosphoribosyl-transferase levels (*Hprt*; Forward Primer 5'-AGCCGACCGGTTCTGTCAT-3'; Reverse Primer 5'-GGTCATAACCTGGTTCATCATCAC-3'; Probe FAM-5'-CGACCCTCAGTCCCAGCGTCGTGAT-3'-TAMRA) or 18S ribosomal RNA (*Rn18s*; assay ID: Mm03928990_g1).

2.12. Western blotting

Protein lysates from liver and BAT were separated by SDS-PAGE, electrotransferred to polyvinylidene difluoride membranes (PVDF; Merck Millipore) with a semidry blotter and probed with the following antibodies against: α -tubulin (1:5000; Sigma; T5168; RRID: AB_330337), β -actin (1:5000; Sigma; A5316; RRID: AB_476743), ACC α (1:1000; Cell Signaling Technology; 3662S; RRID: AB_2219400), AMPK α 1 (1:1000; Merck; 07–350; RRID: AB_310542), AMPK α 2 (1:1000; Merck; 07–363; RRID: AB310553), CPT1A (1:1000; Abcam; Ab128568 RRID:AB_11141632), FAS (1:1000; BD-Biosciences; 610963; RRID: AB_398276), glyceraldehyde-3-phosphate dehydrogenase (GAPDH; 1:5000; Sigma; CB1001; RRID: AB_2107426), *Lipin1* (1:1000; Abcam; Ab70138; RRID: AB_1860796), pAMPK α (Trh172; 1:1000; Cell Signaling Technology; 2535S; RRID: AB_331250), pACC α (Ser79; 1:1000; Cell Signaling Technology; 3661S; RRID: AB_330337) and UCP1 (1:10000; Abcam; ab10983; RRID: AB_2241462) as previously described [11,12,14–17,19]. Primary antibodies were incubated with the following secondary antibodies: polyclonal goat anti-rabbit immunoglobulin/HRP

(1:5000; Dako; P0448; RRID: AB_2617138) and polyclonal rabbit anti-mouse immunoglobulin/HRP (1:5000; Dako; P0260; RRID: AB_2636929). Autoradiographic films (Fujifilm) were scanned, and band signals were quantified by densitometry using ImageJ-1.44 software (NIH) as reported [11,12,14,15,17,19]. Values were expressed relative to α -tubulin, β -actin or GAPDH. Representative images for all proteins are displayed, with all bands in each picture derived from the same gel, although they could be spliced for clarity. A black line was inserted on the immunoblots when samples were loaded on the same gel, but not side by side.

2.13. Statistical analysis

Data are expressed as mean \pm SEM; when data are normalized, they are expressed as a percentage of the appropriate controls. Statistical significance was assessed using two-sided Student's t-test (for comparison of two groups), two-way ANOVA, or Mixed-effect analysis (when data were missed), followed by Sidak or Bonferroni's multiple comparisons (for comparison involving more than two groups) or ANCOVA (calorimetric analyses and correlation between triglycerides vs. body weight). $P < 0.05$ was considered significant. Data analysis was performed using Prism 8.0.2 Software (GraphPad).

3. RESULTS

3.1. SF1 neurons highly expressed AMPK γ 2

Firstly, we aimed to investigate the expression of AMPK γ subunits in SF1 neurons of the VMH. Analysis of the *HypoMap* dataset (<https://cellxgene.cziscience.com/>) [20] showed that neurons expressing *Nr5a1* (which encodes SF1) are highly enriched in *Prkag2* (which codifies AMPK γ 2), but not *Prkag1* and *Prkag3* (which encodes AMPK γ 1 and AMPK γ 3, respectively; Figure 1A). These data indicated that AMPK γ 2 is predominantly expressed in that neuronal population of the VMH.

To generate AMPK γ 2 knockout mice in SF1 neurons, SF1-Cre mice [11,12] were crossed with AMPK γ 2-floxed mice which display a floxed exon 6 [8] (Figure 1B). Selective breeding and genotyping produced AMPK γ 2^{fl/fl} (littermate controls) and SF1-Cre AMPK γ 2^{fl/fl} (knockout) animals, with a truncated CBS1 (Figure 1C). To morphologically validate Cre-mediated recombination, we crossed AMPK γ 2^{fl/fl} and SF1-Cre AMPK γ 2^{fl/fl} animals with reporter floxed Ai14-tdTomato mice. This approach allowed us to observe that SF1-Cre-positive animals exhibited tdTomato fluorescence in the majority of the VMH (Figure 1D), pituitary, adrenal, and gonads (Suppl. Fig. 1A), as well as decreased levels of *Prkag2* in ovary and adrenal and a non-significant trend in testis and pituitary (Suppl. Fig. 1B). The validation of AMPK γ 2 deletion was confirmed through in situ hybridization using BaseScope. A specific probe for the *Prkag2* gene, covering the floxed exon 6, was used to assess expression levels in the hypothalamus of SF1-Cre AMPK γ 2^{fl/fl} and AMPK γ 2^{fl/fl} animals. In AMPK γ 2^{fl/fl} animals, AMPK γ 2 expression (red dots) was observed in the VMH, ARC, and surrounding areas (Figure 1E left; 1F top and 1G top). However, SF1-Cre AMPK γ 2^{fl/fl} animals showed almost complete absence of red dots in the VMH, while normal expression was found in the ARC and areas outside the VMH (Figure 1E right; 1F bottom and 1G bottom). The few red dots found inside the VMH (Figure 1E right, black arrowhead) were likely originated from cell types other than SF1. Overall, this evidence validated our strategy to genetically delete AMPK γ 2 in SF1 neurons.

3.2. Loss of AMPK γ 2 in SF1 neurons increased body weight

We then investigated how AMPK γ 2 deletion in SF1 neurons affected body energy balance. Both male and female SF1-Cre AMPK γ 2^{fl/fl} mice

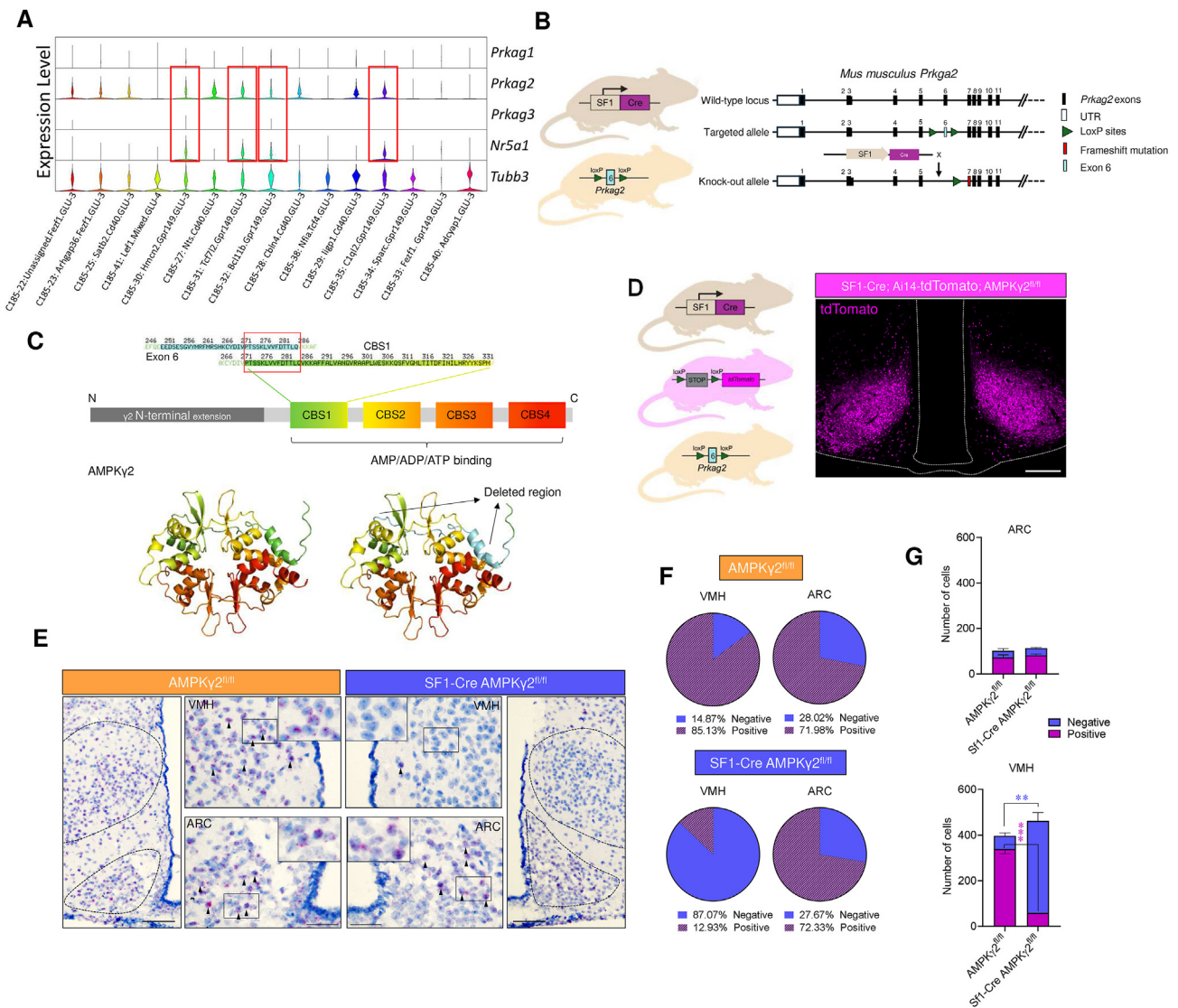


Figure 1: Genetic ablation of AMPK γ 2 in SF1 neurons. (A) Violin plots depicting expression of the different AMPK gamma isoforms, *Prkag1*, *Prkag2*, and *Prkag3*, across ventromedial nucleus of the hypothalamus (VMH) neuronal clusters identified by *Steuernagel et al.* [20]. A total of 33694 neurons were divided into 15 clusters and AMPK gamma isoforms expression was compared to the neuronal marker *Tubb3* and *Nr5a1*, a canonical marker of the VMH. The width of the violin plot indicates the frequency of cells given at the different expression levels, where *Prkag2* shows continuous, high expression in the different VMH neuronal clusters. (B) Graphical scheme showing AMPK γ 2^{fl/fl} mice in which exon 6 (light blue) of *Prkag2* is flanked by loxP sites (dark green), were bred with mice carrying a transgene for Cre expression (purple) under the control of SF1 promoter (beige). Excision of the exon 6 leads to a frameshift mutation (red) downstream of exon 6. Cre positive mice (SF1-Cre AMPK γ 2^{fl/fl}) and Cre negative mice (AMPK γ 2^{fl/fl}) were used in the different analyses. (C) Upper: Graphical scheme showing exon 6 region (blue) in *Prkag2* and the corresponding region of the CBS1 domain on AMPK γ 2 (green); red square highlights the part of the exon 6 that codifies for CBS1. Lower: 3D structure of AMPK γ 2 retrieved from AlphaFold (AF-Q91WG5-F1-v4). Very low probability predictions (Plddt < 50) are not displayed for clarity. The approximate resulting area deleted in SF1-Cre AMPK γ 2^{fl/fl} animals is highlighted in blue. (D) Left: Graphical scheme of the crossing strategy between SF1-Cre mice, AMPK γ 2^{fl/fl} mice, and Ai14-tdTomato mice. Right: Representative confocal image of the hypothalamus depicting tdTomato immunoreactivity (pink) in SF1-positive neurons, mostly located in the VMH, for SF1-Cre-Ai14; AMPK γ 2^{fl/fl}. Scale bar 200 μ m. (E) Brightfield images of in situ hybridization using *BaseScope* probe targeting the exon 6 of *Prkag2* (red) in the hypothalamus of AMPK γ 2^{fl/fl} and SF1-Cre AMPK γ 2^{fl/fl} mice. Zoomed images depict areas in ventromedial nucleus (VMH) and arcuate nucleus (ARC) of the hypothalamus. Blue denotes nuclei stained by hematoxylin; black head arrows depict positive cells for the exon 6 of *Prkag2*. Scale bars 100 μ m for lateral images and 50 μ m for inner images. (F) Quantification of relative number of positive and negative cells shown as their % in respect to total number of cells, from images in (E), for VMH and ARC in both AMPK γ 2^{fl/fl} (n = 2) and SF1-Cre AMPK γ 2^{fl/fl} mice (n = 4). Between 3 and 4 brain slices were analyzed and quantified for each animal. (G) Quantification of the total number of positive and negative cells from images in (E), for VMH and ARC in both AMPK γ 2^{fl/fl} (n = 2) and SF1-Cre AMPK γ 2^{fl/fl} mice (n = 4). Between 3 and 4 brain slices were analyzed and quantified for each animal. Data expressed as mean \pm SEM. **P < 0.01, and ***P < 0.001 vs. control. Statistical significance was assessed by Student's t-test. (For interpretation of the references to colour in this figure legend, the reader is referred to the Web version of this article.)

fed a standard diet exhibited increased body weight, independent of food intake (Figure 2A–B, 2F–G). In fact, when feeding was corrected by body weight, null mice exhibited hypophagia (Figure 2C, H), which was in accordance with the energy expenditure data (see below). These mice also showed higher adiposity, with enlarged subcutaneous

(scWAT), gonadal (gWAT), or visceral (vWAT) white adipose tissue depots (Figure 2D–E, 2I–J). In keeping with the lack of effect of AMPK γ 2 deletion on absolute feeding, hypothalamic mRNA levels of *Agrp*, *Npy*, and *Pomc* were normal in SF1-Cre AMPK γ 2^{fl/fl} male mice (Suppl. Fig. 2A). Glial fibrillary acidic protein (GFAP) protein levels were

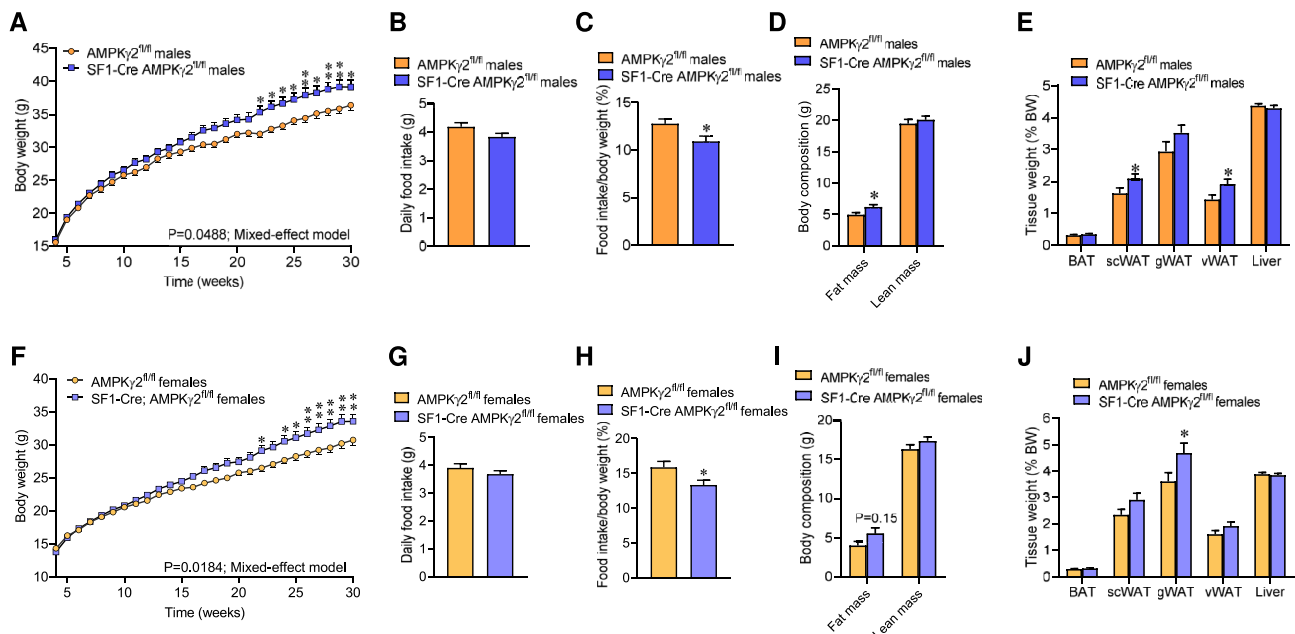


Figure 2: Effect of loss of AMPK γ 2 in SF1 neurons on energy balance. (A–E) Body weight (A; $n = 35$ control and 36 KO), daily food intake (B; $n = 14$ control and 14 KO), food intake normalized by body weight (C; $n = 14$ control and 14 KO), body mass composition by MRI (D; $n = 7$ control and 6 KO), and tissue weight (E; $n = 31$ control and 32 KO; 17–18 weeks old) of control (littermates AMPK γ 2^{fl/fl}) and SF1-Cre AMPK γ 2^{fl/fl} (KO) male mice. (F–J) Body weight (F; $n = 41$ control and 46 KO), daily food intake (G; $n = 18$ control and 20 KO), food intake normalized by body weight (H; $n = 18$ control and 20 KO), body mass composition by MRI (I; $n = 18$ control and 21 KO), and tissue weight (J; $n = 31$ control and 36 KO; 23–24 weeks old) of control and SF1-Cre AMPK γ 2^{fl/fl} female mice. Data are expressed as mean \pm SEM. * $P < 0.05$, and ** $P < 0.01$ vs. AMPK γ 2^{fl/fl}. Statistical significance was assessed by Mixed-effect model (A, F) and Student's *t*-test (B, C, D, E, G, H, I, J).

also unchanged in the ARC and VMH of SF1-Cre AMPK γ 2^{fl/fl} male (Suppl. Figs. 2B–C), indicating that astrocyte cytoarchitecture was not affected by AMPK γ 2 deletion. Overall, these data indicated that, in contrast to the protective effect against weight gain observed with genetic deletion/targeting of AMPK α subunits in the VMH [11,12,15,16], the loss of AMPK γ 2 led to obesity.

3.3. Loss of AMPK γ 2 in SF1 neurons decreased energy expenditure but did not impact glucose homeostasis

We next assessed energy expenditure (EE) by indirect calorimetry in male and female SF1-Cre AMPK γ 2^{fl/fl} mice, given their feeding-independent weight gain phenotype. Analysis of covariance (ANCOVA) of energy expenditure, using body weight as covariate confirmed a significant decrease ($P = 0.0176$; Figure 3A) in male, which we failed to detect in female ($P = 0.7034$; Figure 3D) SF1-Cre AMPK γ 2^{fl/fl} mice. Respiratory exchange ratio (RER; Figure 3B,E) and locomotor activity (LA; Figure 3C,F) remained unaltered in both male and female null mice. Again, this evidence was opposite to that found upon genetic deletion/targeting AMPK α subunits in the VMH, which resulted in increased EE [11,12,15].

AMPK α subunits in SF1 neurons are known to significantly influence glucose homeostasis [12,21]. To investigate the potential role of AMPK γ 2, we conducted a GTT and an ITT test on both male and female SF1-Cre AMPK γ 2^{fl/fl} mice. Our results showed normal glucose tolerance (Figure 3G–H and K–L) and insulin sensitivity (Figure 3I–J and M–N) in both sexes. When the assays were repeated in post-prandial conditions (upon fasting-refeeding challenge; Suppl. Fig. 3A) in male mice, no differences were found in either glucose levels (Suppl. Figs. 3B–C), insulin levels (Suppl. Fig. 3D), or HOMA-IR (Suppl. Fig. 3E). Overall, these results suggested that alterations in AMPK γ 2 function did not impact glucose homeostasis.

3.4. Loss of AMPK γ 2 in SF1 neurons decreased BAT thermogenesis and WAT browning

Hypothalamic AMPK plays a crucial role in regulating BAT thermogenesis and WAT browning, as evidenced by studies demonstrating that the ablation/genetic targeting of AMPK α 1 in SF1 neurons enhances BAT thermogenesis and promotes weight loss [11,12,15,16,22]. Given the observed feeding-independent weight gain in SF1-Cre AMPK γ 2^{fl/fl} mice, we conducted an analysis of BAT thermogenesis and WAT browning in both male and female null mice to further elucidate the mechanisms underlying this phenotype. While body temperature showed no significant differences between genotypes (Figure 4A,J), infrared thermography (IRT) analysis confirmed decreased BAT temperature (Figure 4B–C and 4K–L) and BAT UCP1 protein levels (Figure 4D–E and 4M–N), in both male and female mutants when compared to control littermates. Both sexes also exhibited diminished levels of scWAT browning, as demonstrated by decreased UCP1 staining (Figure 4F–G and 4O–P) and increased adipocyte area (Figure 4H–I and 4Q–R). Altogether, these data indicated that, in contrast to the hyperthermogenic phenotype displayed upon genetic ablation/targeting of AMPK α 1 in SF1 neurons [11,12,15,16,22], loss of AMPK γ 2 led to impaired thermogenesis. We sought to better understand the physiological basis of the observed BAT phenotype. Thus, we examined whether the impact of AMPK γ 2 deficiency in SF1 neurons could be influenced by ambient temperature. This consideration was important because mice are typically housed in non-thermoneutral conditions (22–23 °C), which could lead to baseline BAT activation. Such activation might potentially mask or interfere with the effects of AMPK γ 2 ablation. Firstly, SF1-Cre AMPK γ 2^{fl/fl} male mice were exposed to cold (4 °C) for 6 h (Figure 5A). Null mice showed a similar body (Figure 5B), BAT (Figure 5C–D) and base tail temperature (indicating normal heat

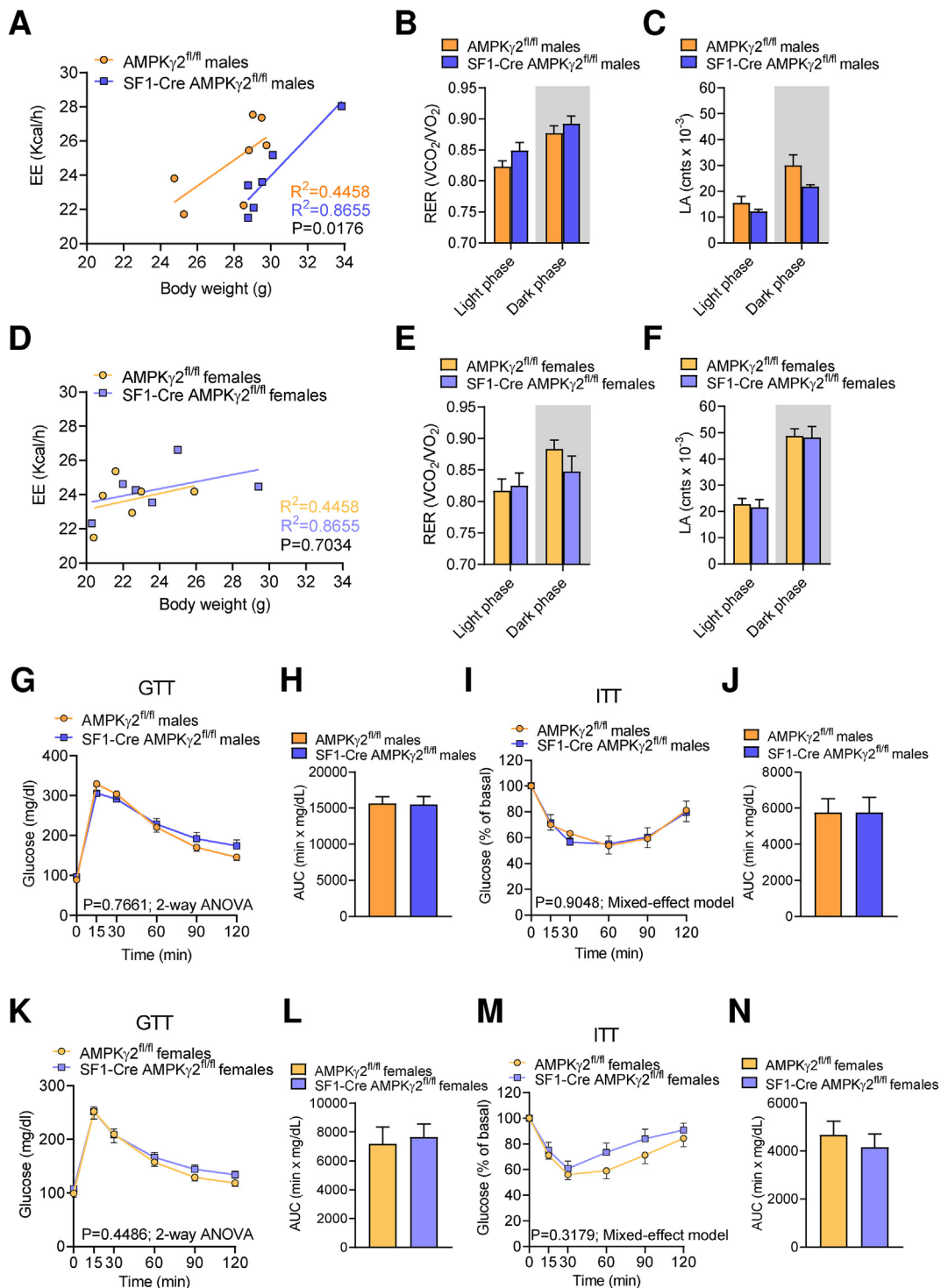


Figure 3: Effect of loss of AMPK γ 2 in SF1 neurons on energy expenditure and glucose homeostasis. (A–C) ANCOVA analysis of 48h total energy expenditure using body weight as a covariate (**A**; $n = 7$ control and 6 KO), daily respiratory exchange ratio (RER, **B**; $n = 7$ control and 6 KO), and total locomotor activity (LA, **C**; $n = 7$ control and 6 KO) of control (littermates AMPK γ 2^{fl/fl}) and SF1-Cre AMPK γ 2^{fl/fl} (KO) male mice. **(D–F)** ANCOVA analysis of 48h total energy expenditure using body weight as a covariate (**D**; $n = 6$ control and 6 KO), RER (**E**; $n = 6$ control and 6 KO), and LA (**F**; $n = 6$ control and 6 KO) of control and SF1-Cre AMPK γ 2^{fl/fl} female mice. **(G–J)** Glucose tolerance test and area under the curve (**G**, **H**; $n = 16$ control and 18 KO), insulin tolerance test, and area under the curve (**I**, **J**; $n = 10$ control and 9 KO) of control and SF1-Cre AMPK γ 2^{fl/fl} male mice. **(K–N)** Glucose tolerance test, area under the curve (**K**, **L**; $n = 16$ control and 21 KO), insulin tolerance test, and area under the curve (**M**, **N**; $n = 10$ control and 16 KO) of control and SF1-Cre AMPK γ 2^{fl/fl} female mice. Data expressed as mean \pm SEM. Statistical significance was assessed by ANCOVA (**A**, **D**), two-way ANOVA or Mixed-effect model (**G**, **I**, **K**, **M**) and Student's *t*-test (**B**, **C**, **E**, **F**, **H**, **J**, **L**, **N**).

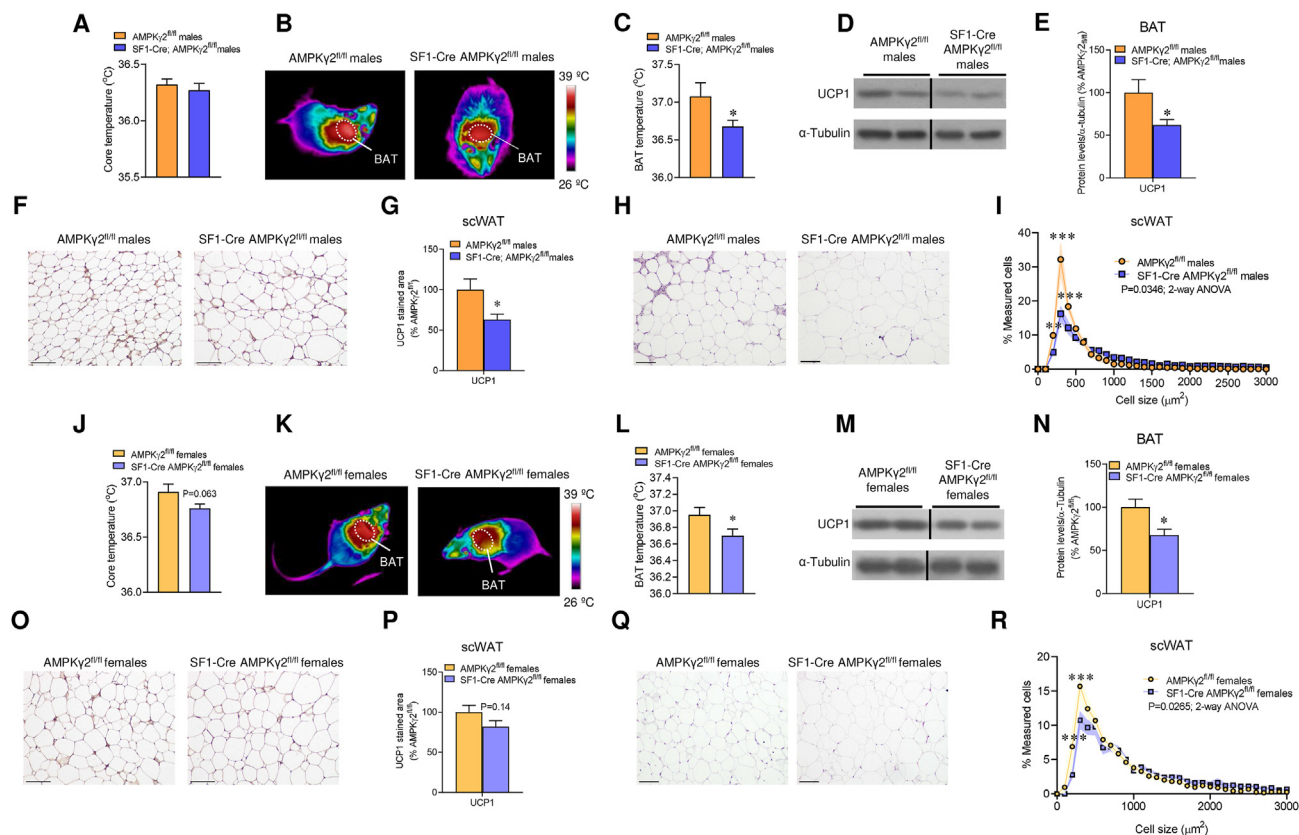


Figure 4: Effect of loss of AMPK γ 2 in SF1 neurons on BAT thermogenesis and WAT browning. (A) Core body temperature of control and SF1-Cre AMPK γ 2^{fl/fl} (KO) male mice (n = 25 control and 26 KO). (B–C) Representative BAT infrared thermographic images (B) and BAT temperature (C; n = 8 control and 16 KO) of control and SF1-Cre AMPK γ 2^{fl/fl} male mice. (D–E) Representative BAT UCP1 western blot images (D) and BAT UCP1 protein levels (E; n = 6 control and 7 KO) of control (littermates AMPK γ 2^{fl/fl}) and SF1-Cre AMPK γ 2^{fl/fl} male mice. α -tubulin was used as control. A black line between the immunoblots depicts samples loaded in the same gel, but not next to each other. (F–G) Representative subcutaneous white adipose tissue (scWAT) immunohistochemistry with anti-UCP1 antibody showing UCP1 staining (F; 20 \times ; scale bar: 20 μ m) and UCP1 stained area (G; n = 11 control and 11 KO) of control and SF1-Cre AMPK γ 2^{fl/fl} male mice. The mean value of each animal was obtained from 2 to 4 photos of each tissue. (H–I) Representative scWAT hematoxylin-eosin staining (H) and proportion of measured cells corresponding to different cell size (μ m²) (I; n = 12 control and 14 KO). The mean value of each animal was obtained from 3 to 4 photos of each tissue, and between 131 (minimum) and 615 (maximum) cells were quantified and classified for each animal. (J) Core body temperature of control and SF1-Cre AMPK γ 2^{fl/fl} female mice (n = 19 control and 25 KO). (K–L) Representative BAT infrared thermographic images (K) and BAT temperature (L; n = 19 control and 25 KO) of control and SF1-Cre AMPK γ 2^{fl/fl} female mice. (M–N) Representative BAT UCP1 western blot images (M) and BAT UCP1 protein levels (N; n = 7 control and 7 KO) of control and SF1-Cre AMPK γ 2^{fl/fl} female mice. α -tubulin was used as control. A black line between the immunoblots depicts samples loaded in the same gel, but not next to each other. (O–P) Representative subcutaneous white adipose tissue (scWAT) immunohistochemistry with anti-UCP1 antibody showing UCP1 staining (O; 20 \times ; scale bar: 20 μ m) and UCP1 stained area (P; n = 15 control and 12 KO) of control and SF1-Cre AMPK γ 2^{fl/fl} female mice. (Q–R) Representative scWAT hematoxylin-eosin staining (Q) and proportion of measured cells corresponding to different cell size (μ m²) (R; n = 16 control and 14 KO). The mean value of each animal was obtained from 3 to 4 photos of each tissue, and between 129 (minimum) and 1024 (maximum) cells were quantified and classified for each animal. Data expressed as mean \pm SEM. *P < 0.05, **P < 0.01, ***P < 0.001 vs. AMPK γ 2^{fl/fl}. Statistical significance was assessed by two-way ANOVA (I, R) and Student's t-test (A, C, E, G, J, L, N, P).

dissipation; Figure 5E). These results demonstrated that, despite a lower basal temperature, null mice were able to defend their body temperature upon cold challenge in similar way than controls. Remarkably, this evidence was also aligned with the fact that, despite decreased basal BAT thermogenesis, SF1-Cre AMPK γ 2^{fl/fl} mice showed normal core temperature. Next, we investigated the opposite paradigm, namely exposure to sub-thermoneutral (26 °C), thermoneutral (30 °C), or supra-thermoneutral (34 °C) conditions during a short (10 min) test (Figure 5F). Considering the high temperatures at which animals were exposed, inner ear temperature was used as a proxy of body temperature. Our data showed that SF1-Cre AMPK γ 2^{fl/fl} mice exhibited lower inner ear (core) temperature at 30 °C and 34 °C (Figure 5G) and normal tail base temperature (Figure 5H–I). These data collectively indicated that male SF1-Cre AMPK γ 2^{fl/fl} mice exhibited impaired basal BAT thermogenesis. However, these mice demonstrated a similar capacity to maintain BAT temperature when

subjected to a cold challenge, while their response to elevated temperatures showed a clear tendency to decreased body temperature. The last results supported that the AMPK γ 2 ablation in SF1 neurons triggered anapyrexia, trying to lower body temperature by simultaneously triggering vasodilation and blocking BAT thermogenesis.

3.5. Loss of AMPK γ 2 in SF1 neurons increased hepatic lipid accumulation

AMPK α 1 deficiency in SF1 neurons has been shown to enhance hepatic *de novo* lipogenesis through parasympathetic nervous system (PSNS) activation [11]. We investigated the effect of AMPK γ 2 deficiency in SF1 neurons on hepatic lipid metabolism. Male SF1-Cre AMPK γ 2^{fl/fl} mice exhibited increased hepatic lipid levels (Figure 6A–B), specifically elevated triglycerides (Figure 6C), but not cholesterol (Figure 6D). Next, we conducted a correlation analysis between hepatic triglycerides and body weight. Notably, null mice demonstrated

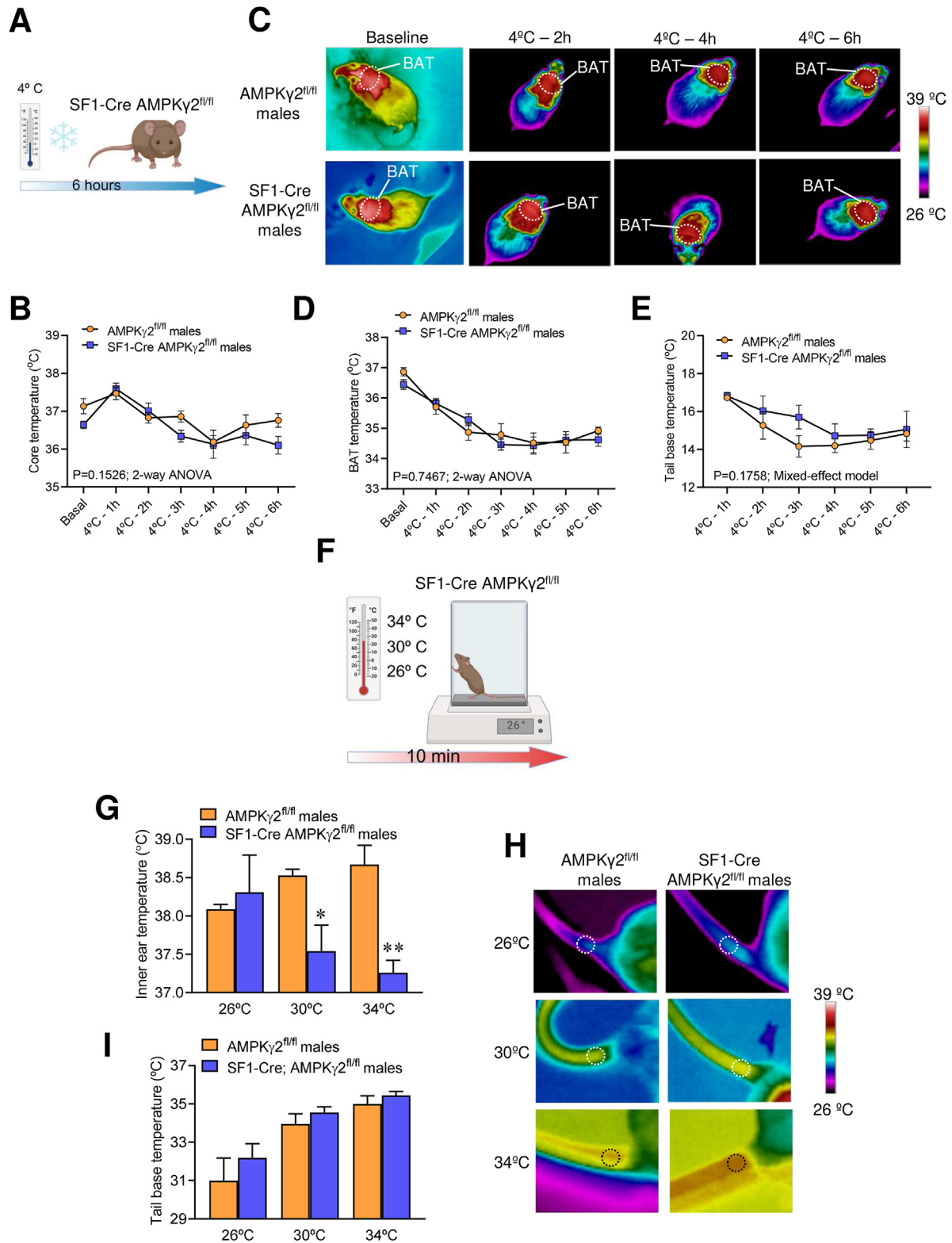


Figure 5: Effect of loss of AMPK γ 2 in SF1 neurons on temperature challenge. (A) Graphical scheme of the cold exposure procedure. (B) Core body temperature change in cold-exposed control (littermates AMPK γ 2^{fl/fl}) and SF1-Cre AMPK γ 2^{fl/fl} (KO) male mice (n = 7 control and 8 KO). (C–E) Representative BAT infrared thermographic images (C; same pair of mice were used for the different time points), BAT temperature (D) and tail base temperature (E) of cold-exposed control and SF1-Cre AMPK γ 2^{fl/fl} male mice (n = 7 control and 8 KO). (F) Graphical scheme of the experimental setup. (G) Inner ear temperature of sub-thermoneutral (26 °C), thermoneutral (30 °C), or supra-thermoneutral (34 °C) exposed control and SF1-Cre AMPK γ 2^{fl/fl} male mice (n = 6 control and 6 KO). (H–I) representative tail base infrared thermographic images (H) and tail base temperature (I) of sub-thermoneutral (26 °C), thermoneutral (30 °C) or supra-thermoneutral (34 °C) exposed control and SF1-Cre AMPK γ 2^{fl/fl} male mice (n = 6 control and 6 KO). Data expressed as mean \pm SEM. *P < 0.05, **P < 0.01 vs. AMPK γ 2^{fl/fl}. Statistical significance was assessed by two-way ANOVA or Mixed-effect model (B, D, E) and Student's t-test (E, G, I).

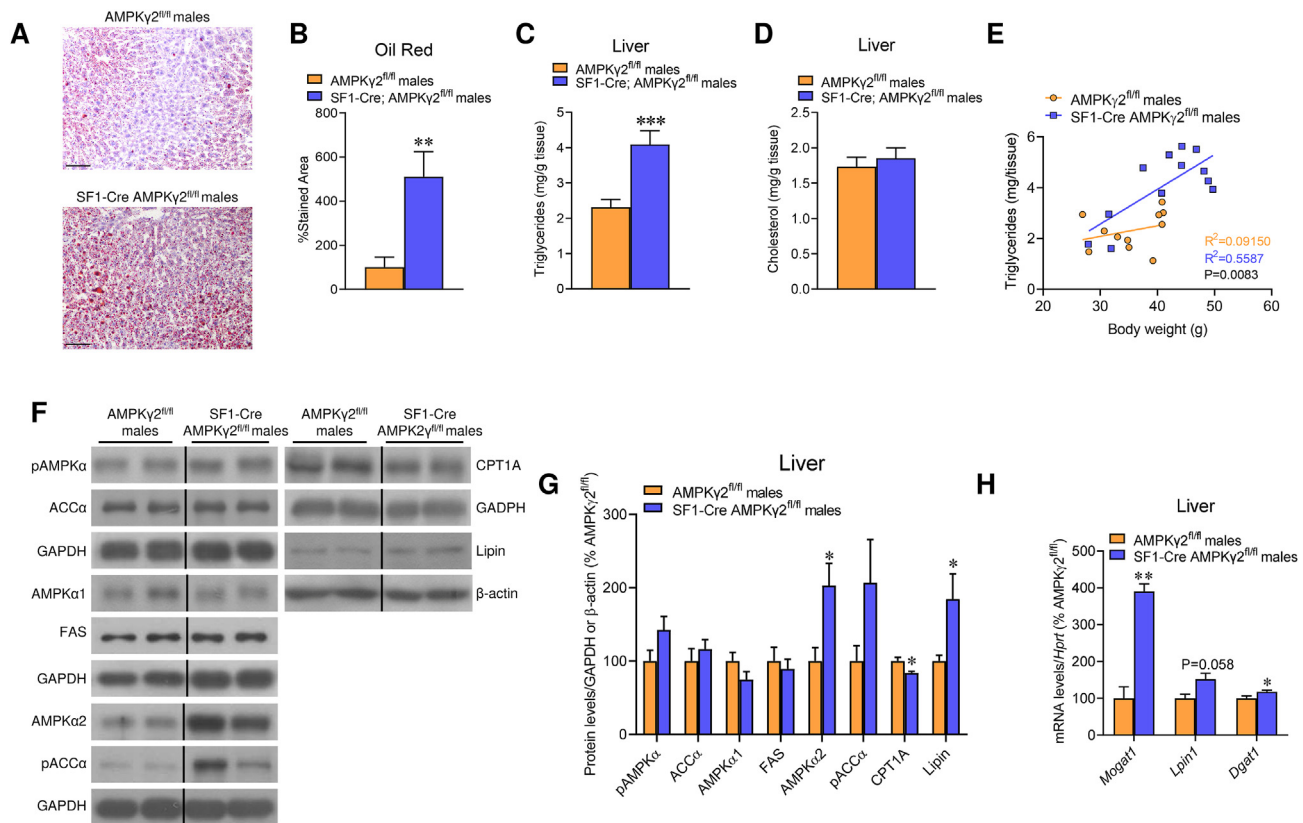


Figure 6: Effect of loss of AMPK γ 2 in SF1 neurons on hepatic lipid metabolism. (A–B) Representative images (A; 20 \times ; scale bar: 40 μ m) of Oil Red O staining in liver samples and percentage of stained area (B) of control (littermates AMPK γ 2^{fl/fl}) and SF1-Cre AMPK γ 2^{fl/fl} male mice (n = 11 control and 12 KO). (C–E) Hepatic triglycerides content (C), cholesterol content (D) and correlation between hepatic triglycerides and body weight (E) of control and SF1-Cre AMPK γ 2^{fl/fl} male mice (n = 11 control and 12 KO). (F–G) Representative liver pAMPK α , ACC α , AMPK α 1, FAS, AMPK α 2, pACC α , CPT1A and Lipin western blot images (F) and quantification of their protein levels (G) in control and SF1-Cre AMPK γ 2^{fl/fl} male mice (n = 7 control and 6–7 KO). GAPDH and β -actin (for Lipin exclusively) were used as control. A black line between the immunoblots depicts samples loaded in the same gel, but not next to each other. (H) Liver mRNA levels of triglyceride synthesis enzymes (*Mogat1*, *Dgat1*, and *Lpin1*; n = 11 control and 12 KO). *Hprt* was used as the housekeeping gene. Data expressed as mean \pm SEM. *P < 0.05, **P < 0.01, and ***P < 0.001 vs. AMPK γ 2^{fl/fl}. Statistical significance was assessed by Student's t-test (B, C, D, G, H) and ANCOVA (E). (For interpretation of the references to colour in this figure legend, the reader is referred to the Web version of this article.)

significantly elevated lipid content even when matched for body weight with controls (P = 0.0083; Figure 6E). This result underscores the genotype-specific effect on hepatic lipid accumulation, independent of overall body mass. While the expression of *de novo* lipogenesis enzymes (AMPK, ACC, and FAS; Figure 6F–G) remained unchanged, the expression of triglyceride synthesis enzymes (MGAT, DGAT, and Lipin, encoded by *Mogat1*, *Dgat1*, and *Lpin1*, respectively; Figure 6F–H) was significantly increased in male null mice. Moreover, hepatic protein levels of CPT1A were significantly reduced (Figure 6F–G). These findings suggested that AMPK γ 2 deficiency in SF1 neurons primarily increased triglyceride synthesis, rather than *de novo* lipogenesis, and reduced lipid oxidation in the liver, leading to hepatic lipid accumulation.

3.6. Loss of AMPK γ 2 in SF1 neurons exacerbated obesity upon HFD

Finally, considering the prone-obese phenotype of SF1-Cre AMPK γ 2^{fl/fl} mice under regular chow, we investigated whether HFD might worsen it. Our data showed that male SF1-Cre AMPK γ 2^{fl/fl} mice fed a HFD (Figure 7A) showed feeding independent weight gain (Figure 7B–C), increased adiposity (Figure 7D), reduced BAT thermogenesis (Figure 7E–F) and a tendency to decrease UCP1 levels in BAT (Figure 7G–H), despite normal glucose tolerance (Figure 7I–J) and insulin sensitivity (Figure 7K–

L) when compared to control littermates. Overall, this evidence indicated that loss of AMPK γ 2 in SF1 neurons promotes obesity due to impaired BAT thermogenesis independently of diet.

4. DISCUSSION

AMPK is a cellular gauge that is activated in conditions of low energy, increasing energy production, and reducing energy-wasting [1,2,23–29]. In the hypothalamus, the AMPK pathway is a canonical route regulating energy homeostasis, by integrating peripheral signals, such as hormones and metabolites with neuronal networks [1,2,30]. Current evidence has linked hypothalamic AMPK α 1 and AMPK α 2 subunits with: (i) the homeostatic regulation of feeding, as well as food preference [31–35], (ii) muscle metabolism [36,37], (iii) hepatic function [38], (iv) glucose homeostasis [12,21,39,40], (v) BAT thermogenesis and browning of WAT [12,17,22,38,41] and (vi) the inflammatory response [19,42]. Current data show that mice lacking AMPK α 1 in SF1 neurons are leaner and protected against obesity [11,12] and that genetic targeting of hypothalamic AMPK α 1 in SF1 neurons of the VMH using a small extracellular vesicles (sEVs)-based approach is a promising strategy for obesity treatment [15,16].

Besides the relevance of AMPK α catalytic isoforms, the regulatory β and γ isoforms may also play a significant role in energy balance. The

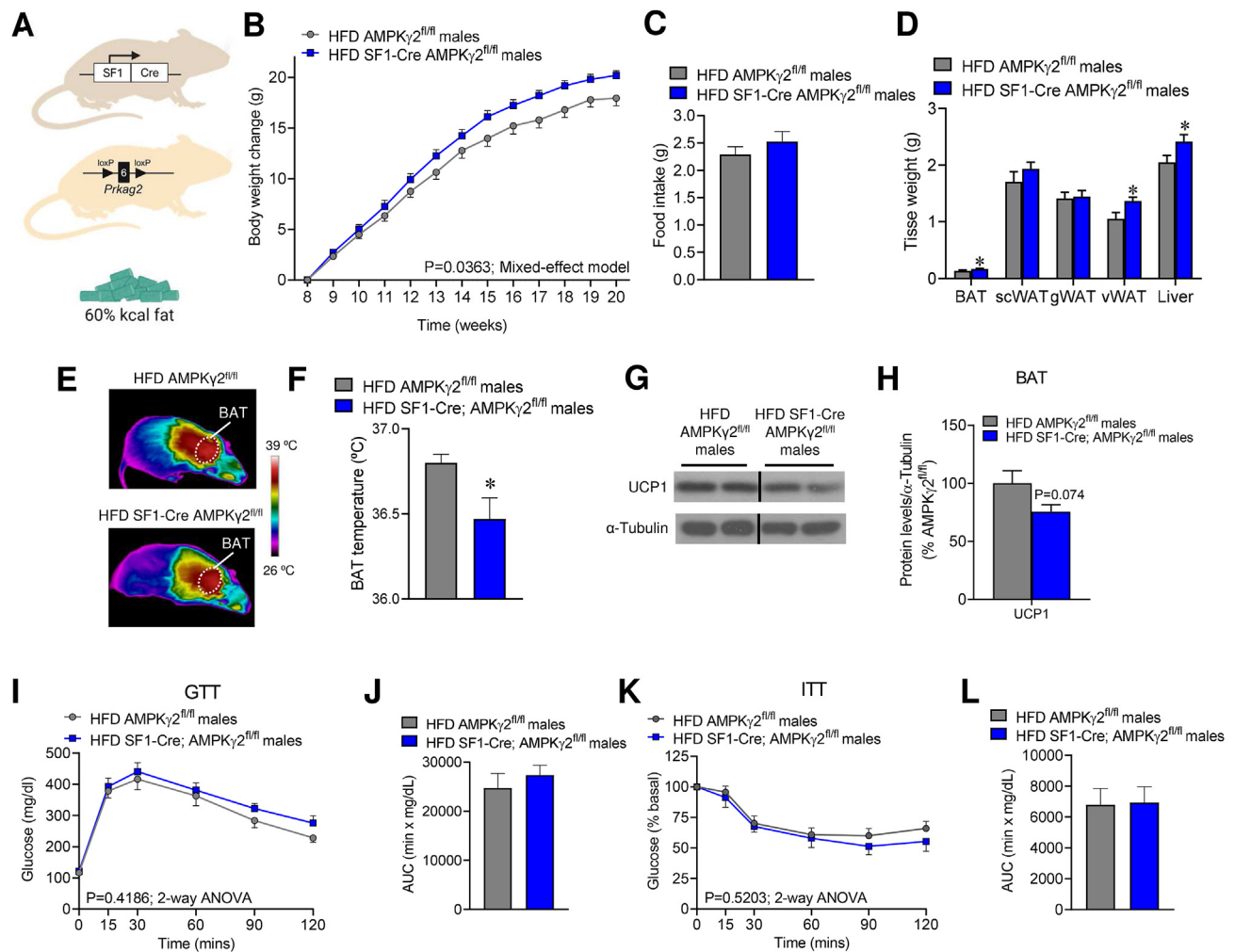


Figure 7: Effect of loss of AMPK γ 2 in SF1 neurons in HFD. (A) Graphical scheme. (B–D) Body weight change after high-fat diet (HFD) exposure (B; n = 30 control and 28 KO), daily food intake (C; n = 13 control and 10 KO), and tissue depot mass (D; n = 18 control and 21 KO) of HFD control (littermates AMPK γ 2^{fl/fl}) and HFD SF1-Cre AMPK γ 2^{fl/fl} (KO) male mice. (E–F) Representative BAT infrared thermographic images (E) and BAT temperature (F; n = 12 control and 10 KO) of HFD control and HFD SF1-Cre AMPK γ 2^{fl/fl} male mice. (G–H) Representative BAT UCP1 western blot images (G) and BAT UCP1 protein levels (H; n = 7 control and 7 KO) of HFD control and HFD SF1-Cre AMPK γ 2^{fl/fl} male mice. α -tubulin was used as control. A black line between the immunoblots depicts samples loaded in the same gel, but not next to each other. (I–L) Glucose tolerance test and area under the curve (I, J; n = 11 control and 5 KO), insulin tolerance test, and area under the curve (K, L; n = 9 control and 5 KO) of HFD control and HFD SF1-Cre AMPK γ 2^{fl/fl} male mice. Data expressed as mean \pm SEM. *P < 0.05, vs. HFD AMPK γ 2^{fl/fl}. Statistical significance was assessed by two-way ANOVA or Mixed-effect model (B, I, K) and Student's t-test (C, D, F, H, J, L).

γ subunit is the primary (and exclusive) “energy sensor”, since it is responsible for binding ATP/AMP and thus plays a key role in the kinase activation, both allosterically and by promoting Thr172 phosphorylation, while preventing its dephosphorylation [2–5]. The γ 2 isoform is primarily expressed in cardiac muscle, where in humans, its mutation results in altered AMPK γ 2 activity, leading to metabolic cardiomyopathies (Wolff-Parkinson-White Syndrome) [6–9]. Mice that were genetically (and globally) modified to express a mutation analogous to one found in humans exhibited increased AMPK activity, obesity, and alterations in insulin secretion [10]. However, there is currently little data on the role of AMPK γ 2 in the hypothalamus. Therefore, the aim of our study was to investigate the metabolic consequences of specific AMPK γ 2 deletion in SF1-expressing neurons, which are crucial for regulating BAT thermogenesis [43,44]. AMPK has been shown to play a major role in energy balance in SF1 neurons [11,12,15,16] and our clustering analysis of the *HypoMap*

dataset [20] showed that AMPK γ 2 is the predominantly expressed AMPK γ subunit within that neuronal population.

Our data revealed that the deletion of AMPK γ 2 in SF1 neurons resulted in an obese phenotype under standard chow conditions, independent of sex and feeding. Mice lacking AMPK γ 2 showed impaired thermogenesis in BAT, reduced browning of scWAT, and males decreased energy expenditure. These findings underscore the critical role of AMPK in regulating thermogenesis within SF1 neurons, although also highlighting the distinct functions of specific AMPK subunits. Thus, whereas the genetic ablation/targeting of AMPK α 1 in SF1 neurons leads to a hyperthermogenic phenotype [11,12,15,16,22], loss of AMPK γ 2 leads to impaired thermogenesis, illustrating the complexity of hypothalamic AMPK's involvement in energy metabolism [1,2,30]. Quite opposite, despite the role of AMPK α 1 and AMPK α 2 in SF1 neurons on glucose levels [12,21], SF1-Cre AMPK γ 2^{fl/fl} displayed normal glucose homeostasis, emphasizing again the differential

function of the AMPK subunits and the impact of their specific targeting on the activity of the $\alpha\beta\gamma$ heterotrimer. In this regard, the cardiac-specific deletion of the $\gamma 2$ subunit using the same AMPK $\gamma 2^{fl/fl}$ mice model (elimination of the exon 6 of *Prkag2* gene; leading to a truncated AMPK $\gamma 2$ subunit) led to normal AMPK $\alpha 1$ and AMPK $\alpha 2$ activities, and increased AMPK $\gamma 1$ function, likely as a compensatory mechanism [8]. In keeping, our preliminary data (not shown) suggests elevated AMPK $\gamma 1$ levels in the VMH of female SF1-Cre AMPK $\gamma 2^{fl/fl}$ mice. However, these results warrant cautious interpretation, as they were derived from western blot analyses of VMH extracts, which contain heterogeneous cell populations beyond SF1 neurons, including other neuronal subtypes and glia. Further cell type-specific and anatomically precise analyses of AMPK $\gamma 1$ expression are necessary to confirm these findings.

These data outline several relevant questions related to the exact role of hypothalamic AMPK. Firstly, why the genetic ablation of two different AMPK subunits within the same neuronal population, namely SF1 cells, yields contracting phenotypes: SF1-Cre AMPK $\alpha 1^{fl/fl}$ mice exhibit a lean, hyperthermogenic phenotype [11,12], while SF1-Cre AMPK $\gamma 2^{fl/fl}$ mice are obese-prone and hypothermogenic. Given the expression profile of AMPK γ subunits in SF1 cells (with AMPK $\gamma 2$ being predominant), it is unlikely that AMPK $\alpha 1$ and AMPK $\gamma 2$ are expressed in distinct populations, since all three subunits are required for the heterotrimer formation, and therefore they may be regulating different neurocircuitries. Secondly, SF1 neurons might comprise heterogeneous subpopulations expressing different AMPK subunit combinations, each with unique downstream targets and functions. This concept of neuronal heterogeneity is not unprecedented, as POMC neurons have been shown to exist in diverse subpopulations with varied functions and targets within the neuroaxis [45,46]. Thus, it could be feasible is that different $\alpha\beta\gamma$ heterotrimers, for example involving AMPK $\alpha 1$ /AMPK $\gamma 2$ or AMPK $\alpha 2$ /AMPK $\gamma 2$ interactions (plus the correspondent β subunit), might be differentially expressed in SF1 subpopulations and might have distinct downstream targets, at molecular and cellular levels [30]. This hypothesis is supported, for example, by the fact that specific virogenetic targeting of AMPK $\alpha 1$ and AMPK $\alpha 2$ within the VMH promotes different phenotypes [12]. Deep analysis of SF1 heterogeneity will be needed to address this. In this regard, considering the expression of SF1 in other tissues, such as testis, ovary, pituitary, and adrenal, we cannot rule out the possibility that AMPK $\gamma 2$ ablation in these tissues could contribute to the observed phenotype. However, our former data using other AMPK α SF1 models showed normal physiological function of those organs [12,15], suggesting that their involvement is unlikely. Thirdly, the role of hypothalamic AMPK extends beyond neurons, requiring investigation in other brain cells, such as astrocytes. Generation of AMPK subunit-null mice in astrocyte-specific Cre lines (e.g., GFAP and glutamate aspartate transporter: GLAST) [47–49] will provide valuable insights into AMPK's hypothalamic functions. Further research into SF1 neuron heterogeneity, its relation with neighboring astrocytes, and AMPK subunit interactions will be crucial to elucidate these complex regulatory mechanisms and their effects on whole-body energy metabolism and other aspects of physiology such as the regulation of circadian rhythms [48,49], where brain AMPK is known to be involved [25].

5. CONCLUSION

Our study reveals that the genetic ablation of AMPK $\gamma 2$ in SF1 neurons of the (VMH) led to a phenotype predisposed to obesity, independent of sex and feeding behavior. This phenotype is marked by a significant reduction of thermogenesis in the BAT and impaired browning in the

WAT, resulting in decreased overall energy expenditure. In addition, our data showing that the AMPK $\gamma 2$ ablation in the SF1 neurons triggers anaprexia suggests that this subunit plays a key integrative role on temperature and energy homeostasis. These findings not only underscore the essential roles of the different AMPK subunits in hypothalamic regulation of energy balance, but also reinforce the idea that by understanding the physiological relevance of AMPK in energy regulation, we can explore novel specific strategies for enhancing metabolic health and combating obesity-related complications.

AUTHOR'S CONTRIBUTIONS

OF-A, AE-S, and VF performed the *in vivo* experiments, analytical methods, and collected the data

OF-A, CLH and CG-C performed the BaseScope analyses

JG-C performed the bioinformatic analyses

ML developed the hypothesis

OF-A and ML coordinated the work, conceived and designed the experiments, and analyzed the data

OF-A, AE-S, VF, IG-G, RN, MT-S, CG-C, CD and ML discussed the data

OF-A and ML made the figures

ML wrote the manuscript; all authors revised and edited the manuscript

ML supervised this work and secured funding

ACKNOWLEDGEMENTS

The research leading to these results has received funding from the Xunta de Galicia (IGG and RN: ED431C 2024/10; IGG: ED431F 2024/14; OFA: predoctoral fellowship ED481A-2019026); Ministerio de Ciencia e Innovación co-funded by the FEDER Program of EU (IGG: PID2022-141115NA-I00; RN: RTI2018-099413-B-I00 and RED2018-102379-T; MT-S: PID2020-118660GB-I00; CD: PID2020-116628GB-I00; ML: PID2021-128145NB-I00 and PDC2022-133958-I00); DZD (CGC), the German Research Foundation DFG under Germany's Excellence Strategy within the framework of the Munich Cluster for Systems Neurology (CGC: EXC 2145 SyNergy—ID 390857198), and Helmholtz Association-Initiative and Networking Fund (CGC); European Research Council (RN: ERC Synergy Grant-2019-WATCH- 810331); 'la Caixa' Foundation (ID 100010434), (ML: LCF/PR/HR19/52160022 and LCF/PR/HR20/52400013); Fundacion Araucaria (ML: PRYGN234908-LOPE). IGG is supported by Ramón y Cajal Contract (RYC2021-031225-I) from the Ministerio de Ciencia e Innovación of Spain. CiMUS was supported by the Xunta de Galicia (2020–2023, ED431G/05). CIBER de Fisiopatología de la Obesidad y Nutrición is an initiative of ISCIII. The funders had no role in study design, data collection and analysis, decision to publish, or preparation of the manuscript.

CREDIT AUTHORSHIP CONTRIBUTION STATEMENT

Óscar Freire-Agulleiro: Writing — review & editing, Visualization, Validation, Methodology, Investigation, Formal analysis, Data curation, Conceptualization. **Ánxela Estévez-Salguero:** Writing — review & editing, Methodology, Investigation, Formal analysis, Data curation. **Vitor Ferreira:** Writing — review & editing, Methodology, Investigation, Formal analysis, Data curation. **Cassie Lynn Holleman:** Writing — review & editing, Methodology, Formal analysis, Data curation. **Julia García-Currás:** Writing — review & editing, Visualization, Methodology, Formal analysis. **Ismael González-García:** Writing — review & editing, Methodology, Investigation, Formal analysis. **Rubén Nogueiras:** Writing — review & editing, Investigation. **Manuel Tena-**

Sempere: Writing — review & editing, Investigation. **Cristina García-Cáceres:** Writing — review & editing, Investigation. **Carlos Diéguez:** Writing — review & editing, Supervision, Investigation. **Miguel López:** Writing — review & editing, Writing — original draft, Visualization, Supervision, Resources, Project administration, Investigation, Funding acquisition, Formal analysis, Conceptualization.

DECLARATION OF COMPETING INTEREST

The authors declare no competing interests.

DATA AVAILABILITY

Data will be made available on request.

APPENDIX A. SUPPLEMENTARY DATA

Supplementary data to this article can be found online at <https://doi.org/10.1016/j.molmet.2024.102091>.

REFERENCES

- [1] Schneeberger M, Claret M. Recent insights into the role of hypothalamic AMPK signaling cascade upon metabolic control. *Front Neurosci* 2012;6:185.
- [2] López M, Nogueiras R, Tena-Sempere M, Dieguez C. Hypothalamic AMPK: a canonical regulator of whole-body energy balance. *Nat Rev Endocrinol* 2016;12(7):421–32.
- [3] Steinberg GR, Carling D. AMP-activated protein kinase: the current landscape for drug development. *Nat Rev Drug Discov* 2019;18(7):527–51.
- [4] Gonzalez A, Hall MN, Lin SC, Hardie DG. AMPK and TOR: the Yin and Yang of cellular nutrient sensing and growth control. *Cell Metabol* 2020;31(3):472–92.
- [5] Steinberg GR, Hardie DG. New insights into activation and function of the AMPK. *Nat Rev Mol Cell Biol* 2023;24(4):255–72.
- [6] Blair E, Redwood C, Ashrafian H, Oliveira M, Broxholme J, Kerr B, et al. Mutations in the gamma(2) subunit of AMP-activated protein kinase cause familial hypertrophic cardiomyopathy: evidence for the central role of energy compromise in disease pathogenesis. *Hum Mol Genet* 2001;10(11):1215–20.
- [7] Arad M, Seidman CE, Seidman JG. AMP-activated protein kinase in the heart: role during health and disease. *Circ Res* 2007;100(4):474–88.
- [8] Cao Y, Bojjireddy N, Kim M, Li T, Zhai P, Nagarajan N, et al. Activation of gamma2-AMPK suppresses ribosome biogenesis and protects against myocardial ischemia/reperfusion injury. *Circ Res* 2017;121(10):1182–91.
- [9] Yavari A, Sarma D, Sternick EB. Human gamma2-AMPK mutations. *Methods Mol Biol* 2018;1732:581–619.
- [10] Yavari A, Stocker CJ, Ghaffari S, Wargent ET, Steeples V, Czibik G, et al. Chronic activation of gamma2 AMPK induces obesity and reduces beta cell function. *Cell Metabol* 2016;23(5):821–36.
- [11] Martinez-Sanchez N, Seoane-Collazo P, Contreras C, Varela L, Villarroya J, Rial-Pensado E, et al. Hypothalamic AMPK-ER stress-JNK1 Axis mediates the central actions of thyroid hormones on energy balance. *Cell Metabol* 2017;26(1):212–229 e212.
- [12] Seoane-Collazo P, Roa J, Rial-Pensado E, Linares-Pose L, Beiroa D, Ruiz-Pino F, et al. SF1-Specific AMPKalpha1 deletion protects against diet-induced obesity. *Diabetes* 2018;67(11):2213–26.
- [13] Gonzalez-Rellan MJ, Fernandez U, Parracho T, Novoa E, Fondevila MF, da Silva Lima N, et al. Neddylation of phosphoenolpyruvate carboxykinase 1 controls glucose metabolism. *Cell Metabol* 2023;35(9):1630–1645 e1635.
- [14] Dragano NRV, Milbank E, Haddad-Tovoli R, Garrido-Gil P, Novoa E, Fondevilla MF, et al. Hypothalamic free fatty acid receptor-1 regulates whole-body energy balance. *Mol Metabol* 2024;79:101840.
- [15] Milbank E, Dragano NRV, Gonzalez-Garcia I, Garcia MR, Rivas-Limeres V, Perdomo L, et al. Small extracellular vesicle-mediated targeting of hypothalamic AMPKalpha1 corrects obesity through BAT activation. *Nat Metab* 2021;3(10):1415–31.
- [16] Milbank E, Dragano N, Vidal-Gomez X, Rivas-Limeres V, Garrido-Gil P, Wertheimer M, et al. Small extracellular vesicle targeting of hypothalamic AMPKalpha1 promotes weight loss in leptin receptor deficient mice. *Metabolism* 2023;139:155350.
- [17] Martínez de Morentin PB, González-García I, Martins L, Lage R, Fernández-Mallo D, Martínez-Sánchez N, et al. Estradiol regulates brown adipose tissue thermogenesis via hypothalamic AMPK. *Cell Metabol* 2014;20(1):41–53.
- [18] Martinez-Sanchez N, Moreno-Navarrete JM, Contreras C, Rial-Pensado E, Ferno J, Nogueiras R, et al. Thyroid hormones induce browning of white fat. *J Endocrinol* 2017;232(2):351–62.
- [19] Seoane-Collazo P, Rial-Pensado E, Estevez-Salguero A, Milbank E, Garcia-Caballero L, Rios M, et al. Activation of hypothalamic AMPK ameliorates metabolic complications of experimental arthritis. *Arthritis Rheumatol* 2022;74(2):212–22.
- [20] Steuernagel L, Lam BYH, Klemm P, Dowsett GKC, Bauder CA, Tadross JA, et al. HypoMap—a unified single-cell gene expression atlas of the murine hypothalamus. *Nat Metab* 2022;4(10):1402–19.
- [21] Quenneville S, Labouebe G, Basco D, Metref S, Viollet B, Foretz M, et al. Hypoglycemia-Sensing neurons of the ventromedial hypothalamus require AMPK-induced Txn2 expression but are dispensable for physiological counterregulation. *Diabetes* 2020;69(11):2253–66.
- [22] López M, Varela L, Vázquez MJ, Rodríguez-Cuenca S, González CR, Velagapudi VR, et al. Hypothalamic AMPK and fatty acid metabolism mediate thyroid regulation of energy balance. *Nat Med* 2010;16(9):1001–8.
- [23] Kahn BB, Alquier T, Carling D, Hardie DG. AMP-activated protein kinase: ancient energy gauge provides clues to modern understanding of metabolism. *Cell Metabol* 2005;1(1):15–25.
- [24] Lage R, Diéguez C, Vidal-Puig A, López M. AMPK: a metabolic gauge regulating whole-body energy homeostasis. *Trends Mol Med* 2008;14(12):539–49.
- [25] Hardie DG, Ross FA, Hawley SA. AMPK: a nutrient and energy sensor that maintains energy homeostasis. *Nat Rev Mol Cell Biol* 2012;13(4):251–62.
- [26] Hardie DG, Schaffer BE, Brunet A. AMPK: an energy-sensing pathway with multiple inputs and outputs. *Trends Cell Biol* 2016;26(3):190–201.
- [27] Carling D. AMPK signalling in health and disease. *Curr Opin Cell Biol* 2017;45:31–7.
- [28] Carling D, Mayer FV, Sanders MJ, Gambin SJ. AMP-activated protein kinase: nature's energy sensor. *Nat Chem Biol* 2011;7(8):512–8.
- [29] Lopez M. AMPK wars: the VMH strikes back, return of the PVH. *Trends endocrinol. Meta* 2018;29(3):135–7.
- [30] Lopez M. Hypothalamic AMPK as a possible target for energy balance-related diseases. *Trends Pharmacol Sci* 2022;43(7):546–56.
- [31] Andersson U, Filipsson K, Abbott CR, Woods A, Smith K, Bloom SR, et al. AMP-activated protein kinase plays a role in the control of food intake. *J Biol Chem* 2004;279(13):12005–8.
- [32] Minokoshi Y, Alquier T, Furukawa N, Kim YB, Lee A, Xue B, et al. AMP-kinase regulates food intake by responding to hormonal and nutrient signals in the hypothalamus. *Nature* 2004;428(6982):569–74.
- [33] Claret M, Smith MA, Batterham RL, Selman C, Choudhury AI, Fryer LG, et al. AMPK is essential for energy homeostasis regulation and glucose sensing by POMC and AgRP neurons. *J Clin Invest* 2007;117(8):2325–36.
- [34] López M, Lage R, Saha AK, Pérez-Tilve D, Vázquez MJ, Varela L, et al. Hypothalamic fatty acid metabolism mediates the orexigenic action of ghrelin. *Cell Metabol* 2008;7(5):389–99.
- [35] Okamoto S, Sato T, Tateyama M, Kageyama H, Maejima Y, Nakata M, et al. Activation of AMPK-regulated CRH neurons in the PVH is sufficient and

- necessary to induce dietary preference for carbohydrate over fat. *Cell Rep* 2018;22(3):706–21.
- [36] Perrin C, Knauf C, Burcelin R. Intracerebroventricular infusion of glucose, insulin, and the adenosine monophosphate-activated kinase activator, 5-aminoimidazole-4-carboxamide-1-beta-D-ribofuranoside, controls muscle glycogen synthesis. *Endocrinology* 2004;145(9):4025–33.
- [37] Xue B, Puliniikunnil T, Murano I, Bence KK, He H, Minokoshi Y, et al. Neuronal protein tyrosine phosphatase 1B deficiency results in inhibition of hypothalamic AMPK and isoform-specific activation of AMPK in peripheral tissues. *Mol Cell Biol* 2009;29(16):4563–73.
- [38] Martínez-Sánchez N, Seoane-Collazo P, Contreras C, Varela L, Villarroya J, Rial-Pensado E, et al. Hypothalamic AMPK-ER stress-JNK1 axis mediates the central actions of thyroid hormones on energy balance. *Cell Metabol* 2017;26(1):212–29.
- [39] McCrimmon RJ, Fan X, Ding Y, Zhu W, Jacob RJ, Sherwin RS. Potential role for AMP-activated protein kinase in hypoglycemia sensing in the ventromedial hypothalamus. *Diabetes* 2004;53(8):1953–8.
- [40] McCrimmon RJ, Shaw M, Fan X, Cheng H, Ding Y, Vella MC, et al. Key role for AMP-activated protein kinase in the ventromedial hypothalamus in regulating counterregulatory hormone responses to acute hypoglycemia. *Diabetes* 2008;57(2):444–50.
- [41] Whittle AJ, S C, L M, Slawik M, Hondares E, Vázquez MJ, et al. Bmp8b increases brown adipose tissue thermogenesis through both central and peripheral actions. *Cell* 2012;149(4):871–85.
- [42] Lopez M, Gualillo O. Rheumatic diseases and metabolism: where centre and periphery meet. *Nat Rev Rheumatol* 2024;20(12):783–94.
- [43] Rouabhi M, Guo DF, Morgan DA, Zhu Z, Lopez M, Zingman L, et al. BBSome ablation in SF1 neurons causes obesity without comorbidities. *Mol Metabol* 2021;48:101211.
- [44] Cardinal P, Andre C, Quarta C, Bellocchio L, Clark S, Elie M, et al. CB1 cannabinoid receptor in SF1-expressing neurons of the ventromedial hypothalamus determines metabolic responses to diet and leptin. *Mol Metabol* 2014;3(7):705–16.
- [45] Leon S, Simon V, Lee TH, Steuernagel L, Clark S, Biglari N, et al. Single cell tracing of Pomc neurons reveals recruitment of 'Ghost' subtypes with atypical identity in a mouse model of obesity. *Nat Commun* 2024;15(1):3443.
- [46] Quarta C, Claret M, Zeltser LM, Williams KW, Yeo GSH, Tschöp MH, et al. POMC neuronal heterogeneity in energy balance and beyond: an integrated view. *Nat Metab* 2021;3(3):299–308.
- [47] Garcia-Caceres C, Quarta C, Varela L, Gao Y, Gruber T, Legutko B, et al. Astrocytic insulin signaling couples brain glucose uptake with nutrient availability. *Cell* 2016;166(4):867–80.
- [48] Gonzalez-Vila A, Luengo-Mateos M, Silveira-Loureiro M, Garrido-Gil P, Ohinska N, Gonzalez-Dominguez M, et al. Astrocytic insulin receptor controls circadian behavior via dopamine signaling in a sexually dimorphic manner. *Nat Commun* 2023;14(1):8175.
- [49] Luengo-Mateos M, Gonzalez-Vila A, Vicente Dragano NR, Ohinska N, Silveira-Loureiro M, Gonzalez-Dominguez M, et al. Hypothalamic astrocytic-BMAL1 regulates energy homeostasis in a sex-dependent manner. *Cell Rep* 2023;42(8):112949.